JMEPEG (2016) 25:2799–2813
DOI: 10.1007/s11665-016-2139-8

1059-9495/$19.00

Influence of Lanthanum on Solidification, Microstructure, and Mechanical Properties of Eutectic Al-Si Piston Alloy

R. Ahmad and M.B.A. Asmael

(Submitted November 10, 2015; in revised form May 11, 2016; published online May 25, 2016)

The effects of Lanthanum (La) concentration on the solidification parameters of the α-Al, Al-Si, and Al-Cu phases and on the microstructure, tensile, and hardness properties of eutectic Al-Si-Cu-Mg alloy were systematically investigated. The solidification parameters were examined using computer-aided cooling curve thermal analysis (CA-CCTA). The cooling curve and microstructure analysis showed that La altered the Si structure. The nucleation and growth temperatures of eutectic Si decreased when 0.3 wt.% La was added, and a high depression temperature was obtained with 1.0 wt.% La. High amounts of La considerably modified the Si structure and decreased the area and aspect ratio by 69.9 and 51%, respectively. The thermal analysis result recorded a faster freezing time with the La addition and a 36% alteration in the secondary dendrite arm spacing. Two secondary or ternary La-rich intermetallic phases were formed with needle- and plate-like structures. Furthermore, the mechanical properties were investigated by hardness and tensile tests with different La concentrations. The addition of small amounts of La (0.1 wt.%) significantly improved the ultimate tensile strength and quality index of the Al-Si-Cu-Mg alloy. In addition, the hardness value of Al-11Si-Cu increased by 7-8% with the increasing amount of La added.

Keywords alloys, lanthanum, mechanical properties, microstructure, thermal analysis

1. Introduction

Al-Si-Cu-Mg alloys exhibit special fluidity and resistance to hot tearing because of their high silicon content and are thus used to produce intricate castings of thin sections. Copper (Cu) and magnesium (Mg) are often added as alloying elements to increase the strength and hardenability of the alloy. Moreover, Al-Si-Cu-Mg alloys exhibit excellent castability and mechanical properties and are popular foundry alloys for industrial applications (Ref 1). These alloys are mainly applied as motor mounts, pistons, cylinder heads, heat exchangers, air conditioners, transmission housings, wheels, and fenders in the automotive industry utilizing recycled (secondary) aluminum because of their high strength at room and high temperature. With the increased use of recycled alloys, alterations in their mechanical properties must be investigated (Ref 2).

In Al-Si-Cu-Mg alloys, copper leads to the formation of the copper intermetallic Cu Al_2. These alloys contain three copper-rich phases: block-like Cu Al_2, eutectic Al-Cu Al_2, and $Al_5Mg_8Cu_2Si_6$. The dissolution rate of the intermetallic compounds is temperature sensitive, and even a 10 °C increase in temperature can affect the optimal solution time and mechanical properties (Ref 1, 3, 4). The structure of the piston alloys significantly affects their physical and mechanical properties. Hence, the macro- and microstructures present in the alloy must be defined and described qualitatively and quantitatively to control the manufacturing process and attain the desired material properties (Ref 5).

Rare earth or mischmetals, such as Ce and La, have been heavily used in the metallurgical industry to improve the strength, malleability, corrosion, oxidation resistance, and creep resistance of various alloys, particularly steel and other iron-based alloys (Ref 6). The further increase in the number of applications of Al-Si alloys depends on the transformation of the Si morphology. Small quantities of certain elements, such as sodium, antimony, and strontium, added to the Al-Si melt could change its needle-shaped silicon crystals into very fine, fibrous, eutectic silicon in a solid solution matrix, thereby improving the mechanical properties of the alloy (Ref 7, 8). The modifying element should exhibit a chemical affinity to form compounds with the precipitating silicon phase at temperatures below the normal eutectic temperature and intermetallic compounds with (and having low solubility in) the solvent α-aluminum phase (Ref 9). La satisfies most of these requirements, whereas Ce and Nd present low solubility in α-aluminum.

Studies have focused on rare earth (RE) elements such as La, which can modify Al-Si eutectic alloys (Ref 10-12). However, other researchers found that La is not related to the modification of the Si morphology and reduction in the strength of the Al-7Si-Mg alloy (Ref 13). In addition, La does not significantly affect Al grain, and the mechanism of the grain-coarsening ability of A356 alloys remains unclear (Ref 14). Yi and Zhang (Ref 15) and Chen and Yang (Ref 16) claimed that the optimal amount of La required to achieve the optimal modification effect is 3.3 wt.%; at this amount, eutectic and primary Si are converted into fine Si particles with small aspect ratios of Al-17Si and Al-25Si alloys. The addition of 3.0 wt.% La into A390 alloy showed a minimal modification effect on the Si phases in the alloy with increasing defects (Ref 17). Thus far, the modification and refining effects of La on Si remain controversial.

The effects of La on the eutectic depression are essential for the Al-Si alloy for evaluation using the thermal analysis cooling curve to assess the quality of the modification. The analysis of

R. Ahmad and **M.B.A. Asmael,** Department of Manufacturing and Industrial Engineering, Faculty of Mechanical and Manufacturing Engineering, Universiti Tun Hussein Onn Malaysia, Parit Raja, 86400 Batu Pahat, Johor, Malaysia. Contact e-mail: roslee@uthm.edu.my.

the temperature-time cooling curve allows metallurgists to monitor the progress of certain metallurgical phase transformations upon additions. Specifically, thermal analysis provides an evaluation of the potential nucleation and modification states of the melt prior to casting (Ref 18). This work aims to investigate the effects of the La concentration on the quality of the modification rate of the Al-Si-Cu-Mg eutectic alloy by monitoring the metallurgical phase transformation parameters during solidification; in particular, the Al-Si and Al-Cu phases of the Al-Si-Cu-Mg eutectic alloy were evaluated through the CA-CCTA technique. The effect of La on the eutectic depression was also determined to assess the quality of modification. Furthermore, metallographic examinations were conducted through scanning electron microscope (SEM) and optical microscope (OM) analyses to correlate the thermal analysis results with the corresponding microstructures. Hardness and tensile tests were also performed to test whether the mechanical properties of the treated alloys deteriorate as a result of the La addition.

2. Experimental Procedure

2.1 Alloy Preparations

Commercial Al-11.7%Si-2Cu-Mg alloy was used as a base alloy for the castings. Different concentrations of the rare earth element La (99.9%; 0.1, 0.3, 0.5, 0.8, and 1.0 wt.%) were added to the molten metal. The melt was stirred for 30 s, and the pouring temperature was set at 750 ± 5 °C.

2.2 Thermal Analysis

A cluster mold with a size of 40 mm × 40 mm was filled with the molten metal. For the analysis, a K-type thermocouple was immersed from the top and placed at the center of the cluster ceramic mold (Fig. 1). Temperature-time data were captured continuously under a dynamic rate of 100 Hz/ch and a resolution of 0.01 °C by using the EPAD2-TH8-K module high-speed data acquisition system connected to DEWE Soft 7.5. The curves were smoothed and plotted, and the first and second derivative cooling curves were produced using FlexPro9 data analysis software to analyze the characteristic data (Fig. 2). From the curves and derivatives, the characteristic temperatures were determined for α-Al, Al-Si, and Al-Cu phases (Table 1). The cooling rate for all cooling curves was 1 °C/s.

2.3 Microstructure Analysis

A slow cooling rate is required to obtain a well-defined cooling record by thermal analysis (Ref 19) due to the difficulties of assessing the solidification parameters in a high cooling rate condition. This is because when a molten metal is solidified by a high cooling rate, the latent heat of any reaction in the solidification process is released quickly, and the reaction peaks in the cooling curve and first derivative curve are too difficult to detect (Ref 20). To increase the accuracy of the thermal analysis, a pre-heated thermally insulated ceramic mold was used, as in previous studies, because it has a lower thermal conductivity (Ref 13, 21-23).

Metallographic examinations must be correlated with the solidification characteristics to determine the fundamental relationship between the cooling curve phase characteristics and the cast structure. All microstructure samples were cut from the site adjacent to the thermocouple (Ref 18, 24, 25) and prepared using standard grinding polishing procedures. OM and image analysis software were used to measure the area and aspect ratio of the silicon particles. The specimens were examined using SEM with an EDS analyzer.

2.4 Mechanical Properties

For good machinability, samples for the mechanical property testing were produced using gravity permanent metal mold casting (Ref 26). After approximately 5 minutes of dissolution and homogenization, the melt was stirred, skimmed, and carefully poured at 750 ± 5 °C into preheated mild steel molds (500 ± 5 °C/30 min) to fabricate tensile test specimens. The castings were machined and milled to obtain the precise specimen dimensions for the cylindrical tensile test according to ASTM B577M (Ref 13, 21, 27); both cylindrical tensile bars corresponded to ASTM B-108 type tensile bars. SEM was used to examine the fracture surface of the tensile bars. In this work, extensive Vickers hardness measurements were conducted to determine the hardness of each alloy.

3. Results and Discussion

3.1 Thermal Analysis

Cooling curves were plotted for the base alloys (untreated alloys) and those treated with La (0.1, 0.3, 0.5, 0.8, and 1.0

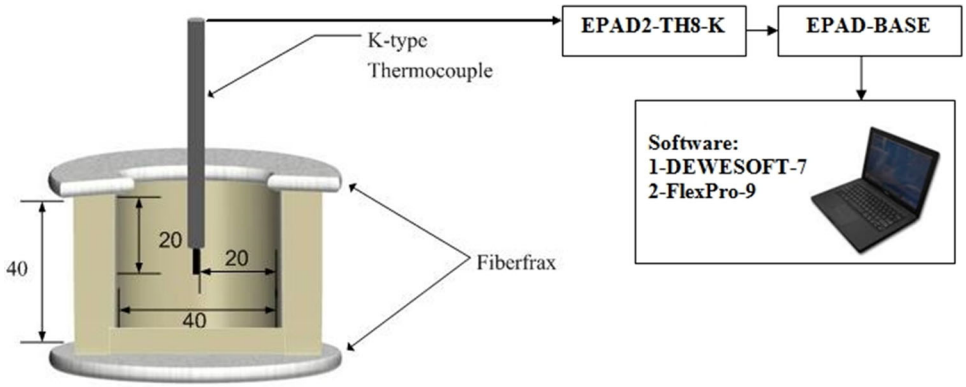

Fig. 1 Thermal analysis set up with a cluster ceramic mold (dimensions in millimeters)

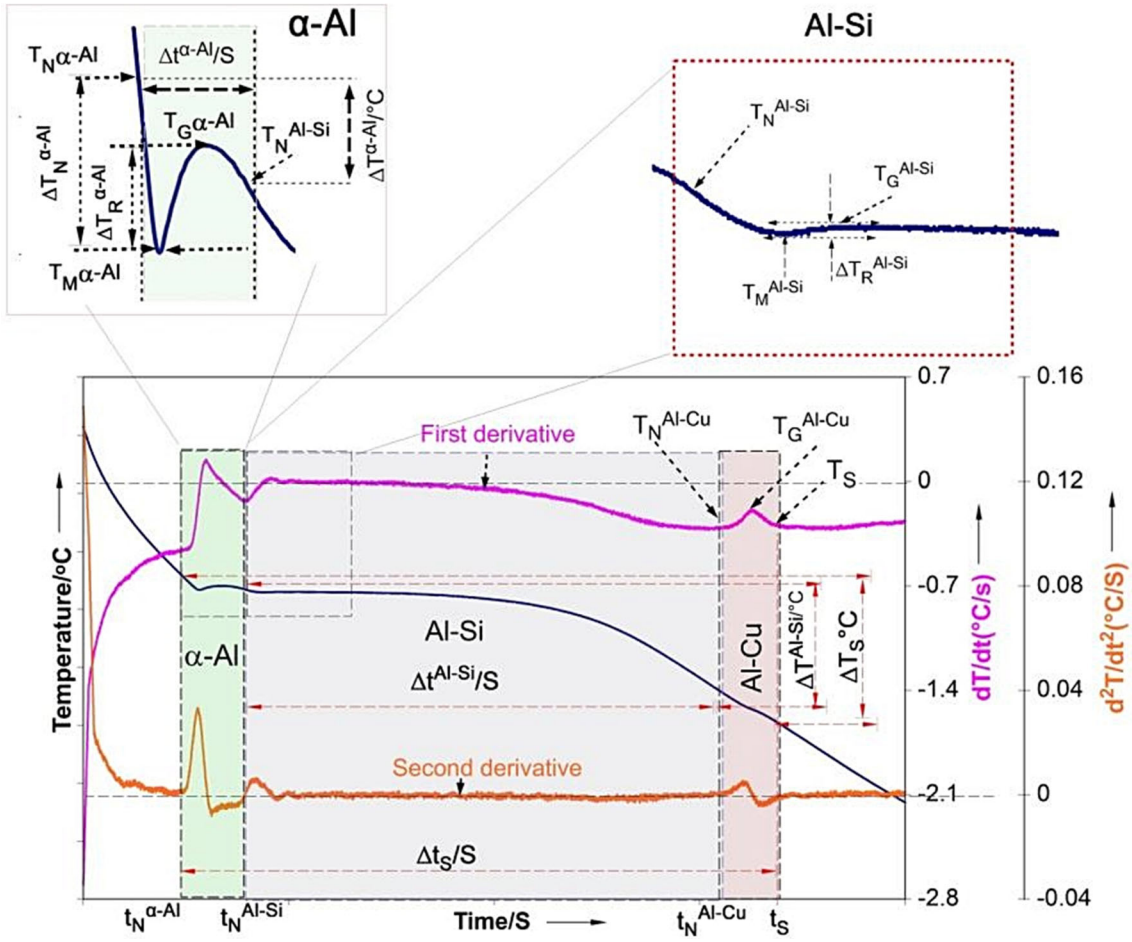

Fig. 2 Cooling curve of Al-11Si-Cu-Mg and its first and second derivatives with three corresponding phase transformations and points of interest

Table 1 Solidification characteristic parameters identified during solidification of α-Al, Al-Si, and Al-Cu phases in Al-Si-Cu alloy

Symbol	Description
$T_N^{\alpha\text{-Al}}$	Nucleation temperature of α-Al, °C
$T_M^{\alpha\text{-Al}}$	Minimum temperature of α-Al, °C
$T_G^{\alpha\text{-Al}}$	Maximum growth temperature of α-Al, °C
$\Delta T_R^{\alpha\text{-Al}}$	Recalescence temperature = ($T_G^{\alpha\text{-Al}} - T_M^{\alpha\text{-Al}}$), °C
$\Delta T_N^{\alpha\text{-Al}}$	Nucleation undercooling temperature = ($T_N^{\alpha\text{-Al}} - T_M^{\alpha\text{-Al}}$), °C
$\Delta T^{\alpha\text{-Al}}$	Solidification temperature range of α-Al phase = ($T_N^{\alpha\text{-Al}} - T_N^{\text{Al-Si}}$), °C
$T_N^{\text{Al-Si}}$	Nucleation temperature of Al-Si, °C
$T_M^{\text{Al-Si}}$	Minimum temperature of Al-Si, °C
$T_G^{\text{Al-Si}}$	Maximum growth temperature of Al-Si, °C
$\Delta T_R^{\text{Al-Si}}$	Recalescence temperature = ($T_G^{\text{Al-Si}} - T_M^{\text{Al-Si}}$), °C
$\Delta T^{\text{Al-Si}}$	Temperature range of Al-S phase = ($T_N^{\text{Al-Si}} - T_N^{\text{Al-Cu}}$), °C
$T_N^{\text{Al-Cu}}$	Nucleation temperature of Al-Cu, °C
$T_G^{\text{Al-Cu}}$	Maximum growth temperature of Al-Cu, °C
$\Delta T^{\text{Al-Cu}}$	Temperature range of Al-Cu phase = ($T_N^{\text{Al-Cu}} - T_S$), °C
T_S	Solidus temperature (end of solidification), °C
ΔT_S	Total temperature range = ($T_N^{\alpha\text{-Al}} - T_S$), °C

wt.%), as shown in Fig. 3. The main cooling curve parameters of all alloys under different La concentrations are presented in Table 2.

3.1.1 α-Al Phase. The solidification of Al-Si casting alloys begins with the nucleation and growth of primary α (Al), followed by the subsequent precipitation of various phases

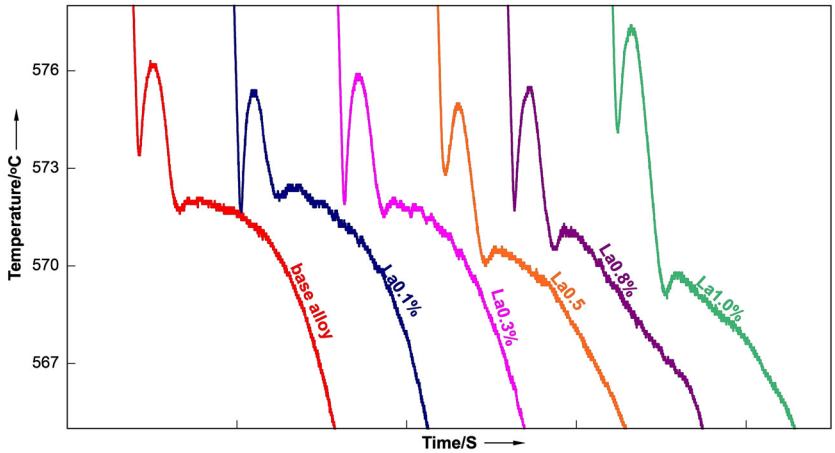

Fig. 3 Cooling curves of Al-11Si-Cu-Mg alloy with and without La addition

Table 2 Solidification parameters of Al-11Si-Cu-Mg alloy with different La concentrations in α-Al, Al-Si, and Al-Cu eutectic phases

		Alloys					
Phase	**Parameters**	**0 wt.% La**	**0.1 wt.% La**	**0.3 wt.% La**	**0.5 wt.% La**	**0.8 wt.% La**	**1.0 wt.% La**
α-Al	$T_N^{\alpha\text{-Al}}$, °C	580.0	578.0	578.9	579.9	578.5	586.3
	t, s	151.2	143.3	166.7	119.6	187.9	190.9
	$T_M^{\alpha\text{-Al}}$, °C	573.4	571.5	571.9	572.8	571.7	574.1
	t, s	170.0	158.8	183.1	140.6	204.1	210.1
	$T_G^{\alpha\text{-Al}}$, °C	576.2	575.4	575.9	575	575.5	577.4
	t, s	207.1	189.2	216.2	174.0	238.4	225.1
Al-Si	$T_N^{\text{Al-Si}}$, °C	573.9	574.2	573.3	573.3	573.4	571.4
	t, s	234.2	211.1	230.4	196.8	263.3	233.4
	$T_M^{\text{Al-Si}}$, °C	571.7	572.1	571.5	570.0	570.5	569.0
	t, s	265.5	263.9	267.7	234.4	299.1	250.4
	$T_G^{\text{Al-Si}}$, °C	572.0	572.5	572.1	570.6	571.0	569.8
	t, s	287.8	293.1	296.6	262.6	324.5	287.3
Al-Cu	$T_N^{\text{Al-Cu}}$, °C	499.1	500.1	500.0	501.0	501.3	502.6
	t, s	941.1	897.0	895.4	887.4	942.2	884.0
	$T_G^{\text{Al-Cu}}$, °C	491.4	496.2	495.7	495.8	496.0	498.8
	t, s	974.5	914.4	907.1	908.9	967.3	925.6
	T_S, °C	483.0	487.5	485.2	486.6	488.0	487.0
	t, s	1009.9	948.0	942.9	941.8	1002.2	987.2

containing the alloying elements (Si, Cu, Mg, etc.). At this first step (nucleation and growth), the grain size of the casting is established. The solidification of clean liquid poses a significant nucleation problem. As the temperature of the liquid decreases, the clustering of atoms produces crystalline regions because of the reduced thermal agitation.

The effects of the La addition on the nucleation $T_N^{\alpha\text{-Al}}$ and growth $T_G^{\alpha\text{-Al}}$ temperatures are shown in Table 2. The $T_N^{\alpha\text{-Al}}$ decreased by 2, 1.1, and 1.5 °C upon the addition of 0.1, 0.3, and 0.8 wt.% La. Increasing the La to 1.0 wt.% caused the nucleation temperature to increase by 6.3 °C compared with that of the base alloys; this finding indicates that the nucleation starts earlier than in the base alloy. However, increasing the La to 0.5 wt.% did not significantly change the nucleation temperature.

An increase in the level of La (0.1-0.8 wt.%) resulted in lower growth temperatures than that in the base alloy. By contrast, 0.1, 0.5, and 0.8 wt.% La decreased $T_G^{\alpha\text{-Al}}$ by 0.7, 1.2, and 0.8 °C, respectively. Moreover, high levels of La (1.0 wt.%) showed different scenarios from other quantities of La additions, in which the growth temperature sharply increased from 575.5 °C for 0.8 wt.% La to 577.4 °C for 1.0 wt.% La.

An analysis of the results of $T_G^{\alpha\text{-Al}}$ and $T_N^{\alpha\text{-Al}}$ revealed another important characteristic, namely, continuous nucleation. This phenomenon occurred when the nucleation temperature $T_N^{\alpha\text{-Al}}$ was higher than the growth temperature $T_G^{\alpha\text{-Al}}$ (Ref 28). Knuutinen et al. (Ref 29) found that the continuous nucleation of the eutectic phase in A356 alloy can be predicted when $T_N^{\alpha\text{-Al}} - T_G^{\alpha\text{-Al}} > 0$. This criterion can also be used for the nucleation of primary aluminum. Moreover, in 1.0 wt.%

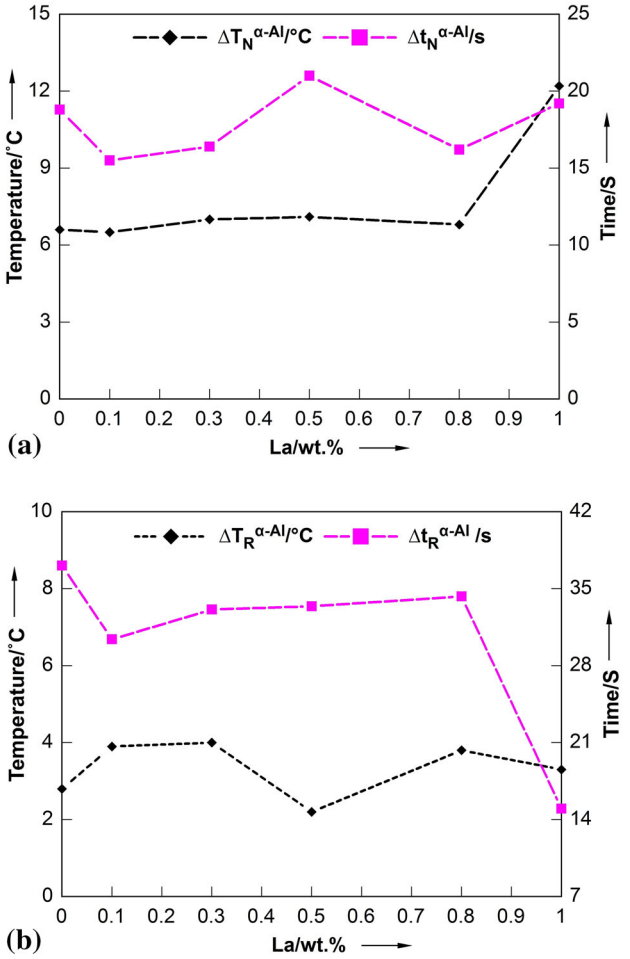

Fig. 4 Variation in (a) nucleation undercooling temperature and time and (b) recalescence temperature and time of α-Al phase in Al-11Si-Cu-Mg alloy as a function of La content

La-containing alloy, the nucleation temperature was approximately 8.9 °C higher than the growth temperature, thereby providing a higher potential for the continuous nucleation of Al dendrites.

The undercooling ($\Delta T_N^{\alpha\text{-Al}}$) and recalescence ($\Delta T_R^{\alpha\text{-Al}}$) temperatures are two important parameters that refer to the nucleation and growth phenomena of aluminum dendrites. These parameters are defined as the differences between the nucleation temperature $T_N^{\alpha\text{-Al}}$ and the minimum temperature $T_M^{\alpha\text{-Al}}$ and between the growth temperature $T_G^{\alpha\text{-Al}}$ and the minimum temperature $T_M^{\alpha\text{-Al}}$, respectively, during a-Al dendrite formation.

Table 2 shows the nucleation undercooling and recalescence temperatures and durations for the base alloy and alloys containing La (Fig. 4). $\Delta T_N^{\alpha\text{-Al}}$ did not change with the increasing amount of La added, whereas high nucleation undercooling was achieved at 1.0 wt.%, as shown in Fig. 4(a). In addition, the undercooling time was minimally affected and decreased with the additions of 0.1, 0.3, and 0.8 wt.% La. The additions of 0.1, 0.3, and 0.8 wt.% La decreased the $\Delta t_N^{\alpha\text{-Al}}$ from 18.8 s in the base alloy to 15.5, 16.4, and 16.2 s, respectively. Moreover, the alloys containing 0.5 and 1.0 wt.% La showed higher $\Delta t_N^{\alpha\text{-Al}}$ of 21 and 19.2 s. However, a longer undercooling time was required at high La levels. As reported by Shabestari et al. (Ref 25), each reaction and evolution requires a driving force. The driving force for the aluminum dendrite nucleation was supplied by the undercooling temperature. Therefore, when a grain refiner is not added to the melt, the liquidus temperature and the minimum temperature considerably differed ($\Delta T_N^{\alpha\text{-Al}} = T_N^{\alpha\text{-Al}} - T_M^{\alpha\text{-Al}}$). This finding indicates the presence of a barrier to nucleation, that casting resulted in relatively coarse grains.

Conversely, when higher levels of nucleates were present in the melt, the barrier for nucleation was reduced, and the dendrite nucleation required a smaller driving force. Therefore, the undercooling temperature decreased, indicating that the casting showed a fine grain structure. Hence, the La addition did not show any grain-refining behavior in the cooling curve or a significant effect on $\Delta T_R^{\alpha\text{-Al}}$, as shown in Fig. 4(b). The recalescence temperature of the base alloy increased from 2.8 to 3.9 °C at all levels of La added, except for 0.5 wt.% La, which obtained a lower temperature increase of 2.2 °C. Alloys supplemented with different levels of La showed shorter recalescence times $\Delta t_R^{\alpha\text{-Al}}$ than the base alloy. This finding could be due to the grain structure of the casting, which is unrelated to the number of nucleation sites in the melt at the liquidus temperature.

In the presence of numerous sites, many grains can be nucleated with minimal undercooling, and a fine-grained structure can be obtained (Ref 25). This finding indicates that nucleation undercooling and recalescence with different La concentrations did not exhibit any grain-refining behavior. Similarly, Zhu et al. (Ref 14) reported that the mechanisms of RE elements in the Al melt are complex and remain challenging. One possible explanation is associated with the liquid-solid freezing range. The entire solidification process was studied by Shabestari et al. (Ref 25) through thermal analysis (Ref 30, 31).

The analysis results of $T_N^{\alpha\text{-Al}}$ and $T_N^{\text{Al-Si}}$ showed the solidification range temperature $\Delta T^{\alpha\text{-Al}}$ of the α-Al phase; this range is the difference between the onset temperature and time of nucleation of the α-Al and Al-Si phases ($\Delta T^{\alpha\text{-Al}} = T_N^{\alpha\text{-Al}} - T_N^{\text{Al-Si}}$). Figure 5 and Table 2 show that the temperature $\Delta T^{\alpha\text{-Al}}$ of the base alloy decreased from 6.1 to 3.8 °C at 0.1 wt.% La and recorded a rapid solidification time ($\Delta t^{\alpha\text{-Al}}$) at 1.0 wt.% La of approximately 45.5 s. In addition, the temperature increased by 14.9 °C with the increasing amount of La added (1.0 wt.%), thereby affecting subsequent stages (Al-Si and Al-Cu). By contrast, low amounts of La do not affect the nucleation or growth temperatures of the Al-Si phase, and the low solid solubility of La in Al influenced the α-Al phase.

3.1.2 Al-Si Phase. The La addition affects the cooling curves, especially in the eutectic reaction region. Table 2 shows that the eutectic temperature decreased upon increasing the La levels up to more than 0.3 wt.%. The temperature $T_G^{\text{Al-Si}}$ decreased to 570.6 °C upon the addition of 0.5 wt.% La and further decreased to 569.8 °C with 1.0 wt.% La, relative to the value of the base alloy. Moreover, the nucleation temperature $T_N^{\text{Al-Si}}$ dropped by 0.7 °C with 0.3 wt.% La and became constant at 0.5 wt.% La compared with that of the base alloy. After the addition of 1.0 wt.% La, the nucleation temperature $T_N^{\text{Al-Si}}$ dropped by 2.5-571.4 °C.

The depression of the eutectic growth temperature as a function of Al-Si-Cu-Mg with different La concentrations was defined by ($\Delta T_G = T_G^{\text{Al-Si}}{}_{unmodified} - T_G^{\text{Al-Si}}{}_{modified}$). The depression started at 0.5 wt.% La, and ΔT_G increased by 1.4 and 2.2 °C after the addition of 0.5 and 1.0 wt.% La, respectively.

The formation of each reaction and evolution requires a driving force. The recalescence temperature $\Delta T_R^{\text{Al-Si}}$ and time $\Delta t_R^{\text{Al-Si}}$ of eutectic arrest were also determined and plotted in Fig. 6. The recalescence temperature $\Delta T_R^{\text{Al-Si}}$ increased with the increasing

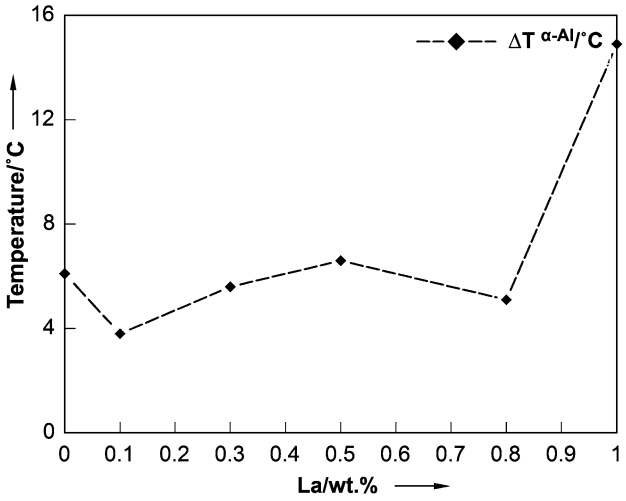

Fig. 5 Variation in the solidification range temperature of the α-Al phase in the Al-11Si-Cu-Mg alloy as a function of the La content

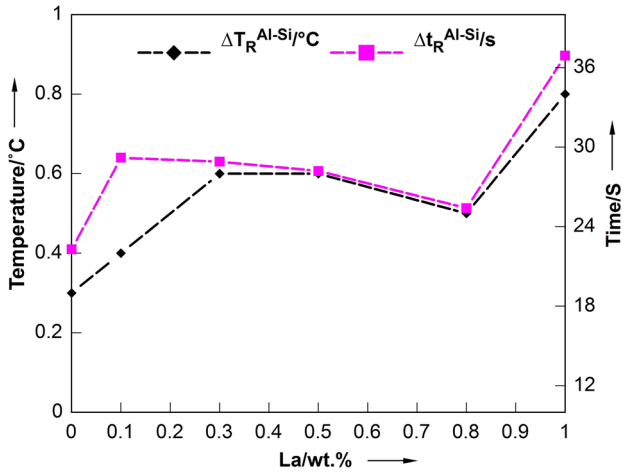

Fig. 6 Variation in the recalescence temperature and time in the Al-Si phase of the Al-11Si-Cu-Mg alloy as a function of the La content

amount of La added. A low recalescence temperature $\Delta T_R^{Al\text{-}Si}$ was recorded in the base alloy, which could be due to the impurity effect of Fe and Mn (Ref 32). By contrast, a recalescence temperature slightly higher by 0.8 °C was obtained with 1.0 wt.% La. In addition, the recalescence time $\Delta t_R^{Al\text{-}Si}$ increased with the increasing La concentration (Fig. 6). An alloy containing 1.0 wt.% La showed a higher eutectic arrest time of 36.9 s compared with that of the base alloy (22.3 s).

The results of the La experiments were compared with the findings on the effects of Sr on Al-11%Si-Cu-Mg (Ref 24, 33) to determine the modification level of Sr, which recorded a growth temperature of 564.1 °C under a cooling rate of 1 °C/s. In addition, a high recalescence temperature and time for complete modification were not achieved after the addition of different amounts of La; these parameters are required to achieve fiber modification upon Sr addition. Similar findings were obtained with Ce addition in Al-11S-Cu-Mg (Ref 23). The effect on the recalescence time may be related to the impingement and coalescence of La particles, resulting in the formation of coarse eutectic Si and the precipitation of the Al-Si-La phase under low nucleation (Ref 23, 34). Moreover, the results show that La acts as a refiner. Similarly, Tsai et al. (Ref 13) reported that the La addition to the hypoeutectic Al-7Si-0.3 Mg alloy decreases the eutectic growth and nucleation temperatures; furthermore, the Si structure was not refined until 1.0 wt.% La was added.

The solidification range for the formation of the Al-Si phase was calculated using the difference in the onset formation of the Al-Si phase and the onset configuration of the Al-Cu phase ($\Delta T_S^{Al\text{-}Si} = T_N^{Al\text{-}Si} - T_N^{Al\text{-}Cu}$) (Ref 23, 31). As illustrated in Fig. 7, the temperature $\Delta T_S^{Al\text{-}Si}$ decreased gradually with the increasing La concentration. The temperature slightly decreased to 74.1 and 73.3 °C in alloys containing 0.1 and 0.3 wt.% La compared to 74.8 °C in the base alloy. A decreasing trend in temperature was observed when the amount of La increased from 0.5 to 1.0 wt.% La, and the lowest temperature ($\Delta T_S^{Al\text{-}Si}$ = 68.8 °C) was obtained at 1.0 wt.%.

An analysis of the solidification parameters of the Al-Si phase shows that La acts as a refiner of eutectic Si. The depression of $T_N^{Al\text{-}Si}$ and $T_G^{Al\text{-}Si}$ increased the recalescence temperature because of the lower solubility of La compared to

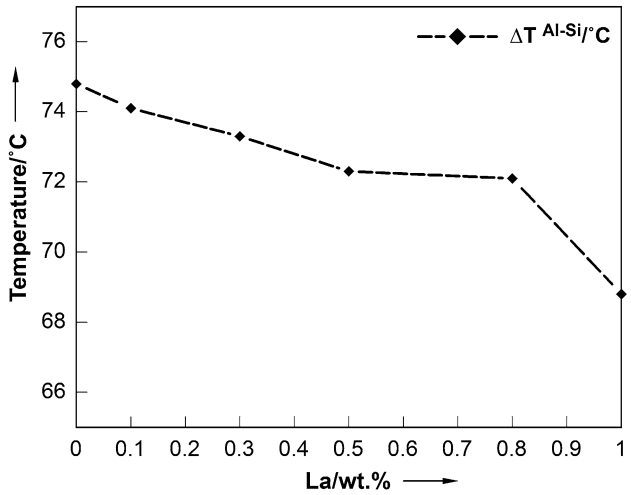

Fig. 7 Variation in the solidification range temperature of the Al-Si phase in the Al-11Si-Cu-Mg alloy as a function of the La content

that of Al but decreased the solidification range temperature of the Al-Si phase (Ref 23, 24). Moreover, the time of solidification of Al-Si $\Delta t_s^{Al\text{-}Si}$ decreased with the increasing La concentration. The distribution of La with respect to time and temperature during the solidification of the Al-Si phase was confirmed by the fact that eutectic Si particles do not have sufficient time to obtain the flake shape and formation of the Al-Si-RE-rich compound at low temperatures (Ref 23).

3.1.3 Al-Cu Phase. The final solidification stage of the Al-11.7%Si-Cu-Mg alloy is the formation of Al-Cu. Copper leads to the formation of three copper-rich phases: block-like Al_2-Cu, eutectic Al-Cu-Al_2, and Al-Mg-Cu-Si (Ref 4, 35, 36). The characteristic parameters of the Al-Cu phase were determined using the first and second derivative curves and are shown in Table 2. From the first derivative result, the growth temperature of the Al-Cu phase ($T_G^{Al\text{-}Cu}$) in the base alloy was lower (499.1 °C) than that in the La-containing alloys. The growth temperature was increased by 4.8 °C after the addition of low levels of La (0.1 wt.%) but was not significantly influenced by 0.8 wt.% La. A high change in $T_G^{Al\text{-}Cu}$ of 7.4 °C was obtained upon the addition of high levels of La. The

addition of La significantly influenced the nucleation temperature of the Al-Cu phase ($T_N^{Al\text{-}Cu}$), as shown in Table 2. With minimal additions of 0.1 and 0.3 wt.% La, the $T_N^{Al\text{-}Cu}$ increased to 500.1 °C. Moreover, the nucleation temperature $T_N^{Al\text{-}Cu}$ continuously increased upon increasing the La from 0.5 wt.% to 1.0 wt.%; a high $T_N^{Al\text{-}Cu}$ of 502.6 °C was observed upon the addition of high levels of La (1.0 wt.%).

The solidification range of the Al-Cu phase obtained using the difference between $T_N^{Al\text{-}Cu}$ and T_S ($\Delta T_S^{Al\text{-}Cu} = T_N^{Al\text{-}Cu} - T_S$) is plotted in Fig. 8. The base alloy showed a high $\Delta T_S^{Al\text{-}Cu}$ temperature change of 16.1 °C, which decreased to 12.6 °C upon the addition of 0.1 wt.% La, which may be due to the influence of this element on the first stage of solidification. A slightly decrease in $\Delta T_S^{Al\text{-}Cu}$ was obtained at 1.0 wt.% La, with a result of 15.6 °C. Moreover, the $\Delta T_S^{Al\text{-}Cu}$ decreased to 14.8, 14.4, 13.3 °C with 0.3, 0.5, 0.8 wt.% La, respectively. When Si particles were modified at high values of La (1.0 wt.%), the time of $\Delta t_s^{Al\text{-}Cu}$ increased to 103 s and that of the unmodified alloy was 68.8 s. The increase in the solidification time in the final stage may be due to Al-Mg-Cu-Si-La phase formation with the Al-Cu phase (Ref 37). Hence, changes in the Al-Cu phase may be due to the formation of the intermetallic compound by La with Al, Cu, Si, and Mg.

Thermal analysis showed that the La addition significantly affected the solidification characteristics of the Al-Si and Al-Cu phases because of the presence of La intermetallic compounds, such as Al-La, Al-Si-La, and Al-Si-La-Cu, with an acicular or flake shape (Ref 14, 15, 38). This finding can be related to the fact that additional atoms of appropriate sizes can induce the nucleation of twins at the solid-liquid interface (Ref 29). In this regard, the system requires a high decrease in temperature as a driving force to initiate nucleation.

3.1.4 Total Solidification Temperature Range and Time. The solidification temperature range (ΔT_S) and time (Δt_s) is defined as the difference between the onset of nucleation of α-Al and the end of solidification T_S. Figure 9 shows the effects of the La solubility. The solidification temperature of the base alloy decreased from 97 to 90.5 °C upon increasing the La level from 0.1 to 0.8 wt.% and then increased to 99.3 °C at 1.0 wt.% La. This increase in temperature may be due to the effect of high La concentrations on the first and final stages of solidification. In addition, intermetallic compounds containing Al and RE exhibited a high melting point and similar lattice constant to that of α-Al (Ref 39).

The total solidification time Δt_s decreased with the increasing La concentration, and a short solidification range of 776.6 s was captured with 0.3 wt.% La (Fig. 9). This finding could be due to an insufficient amount of La (0.1 and 0.3 wt.%) to reduce the nucleation and growth temperatures of the Al-Si phase, as shown in Table 2. After the addition of La to the melt, the element concentrated at the front of the solid-fluid interface during solidification because of its low solid solubility in Al. This phenomenon resulted in the formation of a new phase of Al-La, which is difficult to dissolve at high temperatures. Therefore, the new phase would block the diffusion of Si and increase the equilibrium solubility in the binary Al-Si system; this finding is similar to that reported by Qiu et al. (Ref 40) in treatments with added Sm (samarium). This reduction in the secondary dendrite arm spacing (SDAS) may lead to an improvement in the mechanical properties. Reducing the solidification time positively influences SDAS, which reflects directly on the mechanical properties (Ref 41, 42).

3.2 Microstructure Analysis

The mean solidification phases in the as-cast microstructure of Al-Si-Cu-Mg alloys include acicular and coarse primary Si, large primary α-Al and grain size, and harmful intermetallic phases. Si particles can be modified using an effective modifier element (Ref 43). The sequence of phase precipitation in hypoeutectic Al-Si alloys is summarized in Table 3.

3.2.1 Si Particle Structure. Figure 10 shows optical micrographs of the Al-Si-Cu alloy supplemented with various concentrations of La. The microstructure of the alloys differed in terms of the size of the eutectic silica structure. According to twin plane re-entrant angle edge mechanism (TPRE) theory, facet phases, including primary and eutectic Si crystals of Al-Si alloys, form a coarse structure during solidification (Ref 44). The base alloy showed a flake-plate-like microstructure of Al-11Si-Cu alloy when supplemented with 0.1 and 0.3 wt.% La, as observed in Fig. 10(a) to (c). The size and inter-flake spacing of

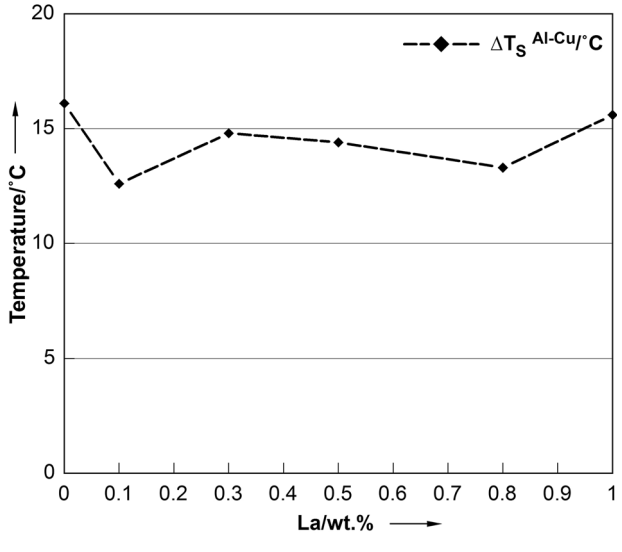

Fig. 8 Variation in the solidification range temperature of the Al-Cu phase in the Al-11Si-Cu-Mg alloy as a function of the La content

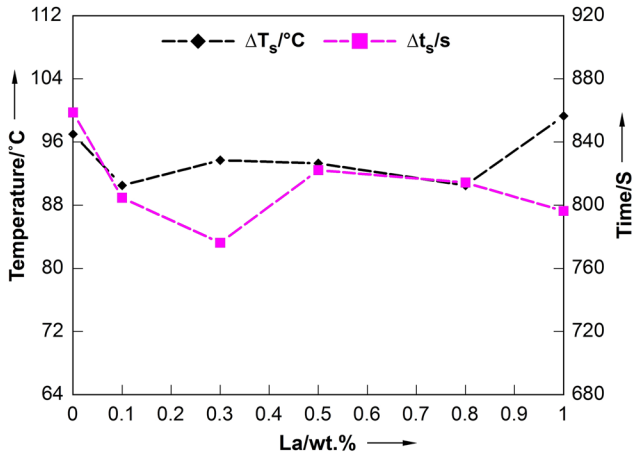

Fig. 9 Variation in the total solidification temperature range and time of Al-11Si-Cu-Mg with different levels of La added

Table 3 Sequence of phase precipitation in hypoeutectic Al-Si alloys (Ref 38)

Temperature, °C	Phases precipitated
650	Primary $Al_{15}(Mn, Fe)_3Si_2$
600	Aluminum dendrites and ($Al_{15}(Mn, Fe)_3Si_2$) and/or Al_5FeSi
550	Eutectic Al + Si and Al_5 $FeSiMg_2Si$
500	$CuAl_2$ and more complex phases

the eutectic Si significantly decreased upon the La addition, during which a fine flake structure was observed. Moreover, the coarse acicular and plate-like eutectic Si structure transformed into a branched structure with the decreasing silica size at 0.5 wt.% La. Furthermore, an alloy with 0.8 wt.% La shows irregular-shaped, longitudinal sharp-edged and rounded structures. The Si structure became smaller in refiner silica particles with a high level of 1.0 wt.% La.

Figure 11 presents the changes in the area and aspect ratio of the Si particles of Al-Si-Cu-Mg supplemented with different La levels. The area and aspect ratio of the base alloy were 69.9 μm^2 and 6, respectively, which decreased to 40 μm^2 and 4.3 for 0.5 wt.% La and to 21.3 μm^2 and 2.9 for 1.0 wt.% La, respectively. From the microstructure results, a 1.0 wt.% La level was considered the optimum for refining the Si structure. Similar results were obtained in the refined Si structure of hypoeutectic and eutectic Al-Si alloys with La and other rare earth metals, such as Yb, Ce, and Y (Ref 13, 21, 23, 29, 45). The mechanism of refinement of the Si crystal can be explained by the impurity-induced twinning model (IIT) theory, which indicates that the atoms of the modification agents can be absorbed on the Si solid-liquid interface and alter the growth mode, which results in the refinement of the Si crystals (Ref 44, 46, 47).

3.2.2 Micrographs of Intermetallics. Figure 12 presents an SEM microanalysis to identify the chemical intermetallic composition of the phases present in the alloy. The La phase appeared (bright gray) needle-like or plate-like and was randomly distributed in the modified Si. The sizes of the La-rich Al-Si-La and Al-Si-Cu-La phases were larger than that of the eutectic Si phase, thereby interrupting the modification. Figure 12 also depicts the interaction between the La-rich phase and the primary Si phase at 1.0 wt.% La as well as the presence of large La-rich platelets and polygons near the polygonal Si crystal. The same result was obtained for La with A390 alloys (Ref 15, 17), and the investigated La compounds interrupted the modification of eutectic Si. The presumed composition of the La-rich phase approximated that of the compounds presented in the EDS analysis (Fig. 12). The reaction of La formed compounds with alloy elements such as Al, Si, Cu, and Mg as well as other compounds, namely, ternary Al-Si-La (needle-like), quaternary Al-Si-Mg-La and Al-Si-Cu-La (plate-like), and quinary Al-Si-Mg-Cu-La (needle-like).

La compounds combined with Al, Cu, and Si were found as long interfaces with eutectic Al-Cu-La-Si (Fig. 13). These compounds were found along the interface of eutectic Cu, Si/α-Al or at the edge of the primary Si crystals. This interface can increase the modification because of twin growth (Ref 44, 46, 47). The modification mechanism of La addition to eutectic Al-11Si-Cu-Mg alloy may be attributed to impurity-induced twinning. The EDS mapping result of La is consistent with that reported by Li et al. (Ref 47, 48). La is a type of surface-active agent. In addition, Lu and Hellawell (Ref 49) proposed the theory that twin growth would be created at the interface when the ratio (atomic radius of the modification elements relative to that of silicon) is close to 1.646. For La, r_{La}/r_{Si} is 1.59, which is close to this values (Ref 13). Hence, Al-Cu-La-Si precipitated after the eutectic reaction of Si and after the formation of Al_2Cu (Ref 17). The La-rich phase was formed in pores and broken structures because of the brittle nature of the phase and the large stresses induced by solidification (Ref 15).

The intermetallic compound is an important component used to modify Si. From the SEM result, the Al-Cu-La-Si observed near the polygonal Si disturbed the Si modification. Similarly, Yi and Zhang (Ref 15) reported that in Al-Cu-La-Si, the La has as adverse effect on the Si structure, as confirmed by the microstructure results. Generally, La is a type of surface-active agent. Therefore, the modification of La on Si crystals can be explained through the mechanism that a modifying agent can be adsorbed onto the growth front and thereby effectively poison the growth steps (Ref 15).

3.2.3 Secondary Dendrite Arm Spacing (SDAS). The effect of the La addition on the SDAS is plotted in Fig. 14. The SDAS decreased with the increasing amount of La, and the SDAS of the base alloy decreased from 55 to 35-40 μm (decreased by 27%). This refinement of the SDAS may be due to the effect of La on the solidification time Δt_s (Ref 50, 51). High levels of La (1.0 wt.%) slightly increased the SDAS compared to the other levels, which may be due to increase in the temperature range of $\Delta T^{\alpha\text{-Al}}$ and ΔT_S with 1.0 wt.% La. Reducing the solidification time positively influenced the SDAS, which reflected directly on the mechanical properties (Ref 41, 42).

As shown in Fig. 9, the La concentration reduced the solidification time Δt_s relative to that of the base alloy. This finding may be due to the solubility of La in the α-Al phase, whereas La had a lower solid solubility than aluminum, meaning that, La concentrates in front of the solid-liquid interface during the growth of α-Al grains due to the segregation, leading to SDAS reduction (Ref 13, 52-54). Moreover, RE metals, such as Ce, Sm, and Er (erbium), refined the SDAS of α-Al according to the fluid interface (Ref 55, 56). As reported by Bolieu (Ref 41, 42), reducing the solidification time positively influenced the SDAS, which reflected directly on the mechanical properties. In addition, the primary Al phase precipitated because the eutectic reaction supplied numerous nucleation cores for the α-Al phase (Ref 39).

3.3 Mechanical Properties

3.3.1 Tensile Test. The variations of the tensile properties such as the UTS, elongation to fracture, and quality index of the analyzed alloys are shown in Fig. 15. The result shows an improvement in the UTS, with small amounts of 0.1 and 0.3 wt.% La increased the tensile strength from 203.4 MPa for the base alloy to 206.5 and 206.3 MPa, respectively. Upon the addition of 0.5, 0.8, and 1.0 wt.% La, the UTS decreased to 194.4, 171.5, and 191.5 MPa, respectively, but no improvement in the UTS was obtained. This finding is attributed to the lesser potential of these additions as a result of gas pickup, porosity formation, and intermetallic compounds. In addition to the porosity and intermetallic formation, the 0.8 wt.% La-containing alloy exhibited a lower UTS compared to the 1.0 wt.% La

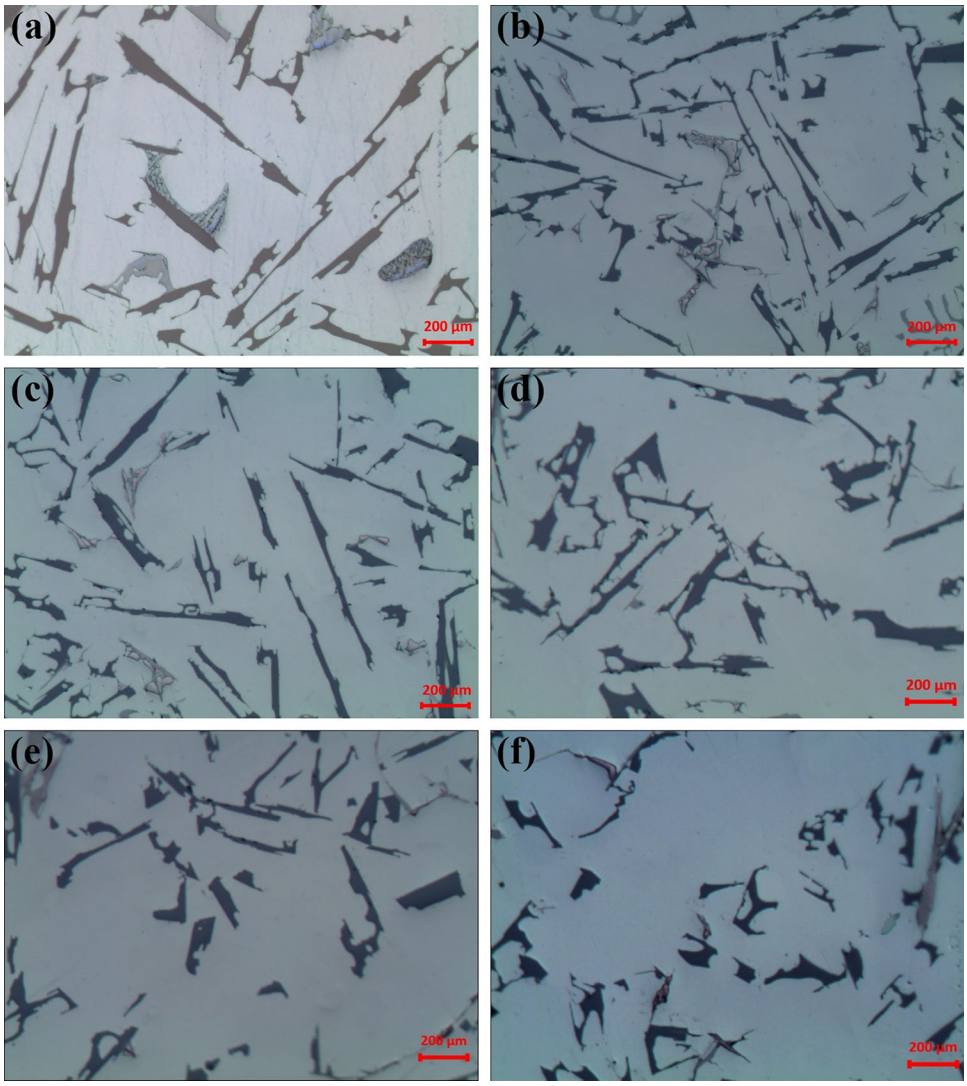

Fig. 10 Microstructures of thermal analysis test samples of Al-11Si-Cu-Mg with different La concentrations: (a) base alloy, (b) 0.1 wt.% La, (c) 0.3 wt.% La, (d) 0.5 wt.% La, (e) 0.8 wt.% La, and (f) 1.0 wt.% La

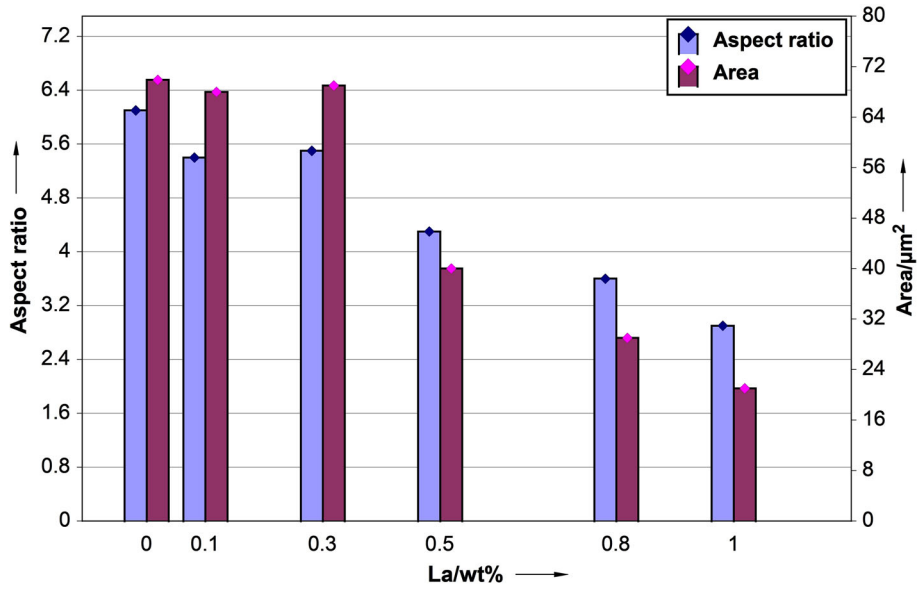

Fig. 11 Image analysis of eutectic silicon particles of base alloy with different La levels

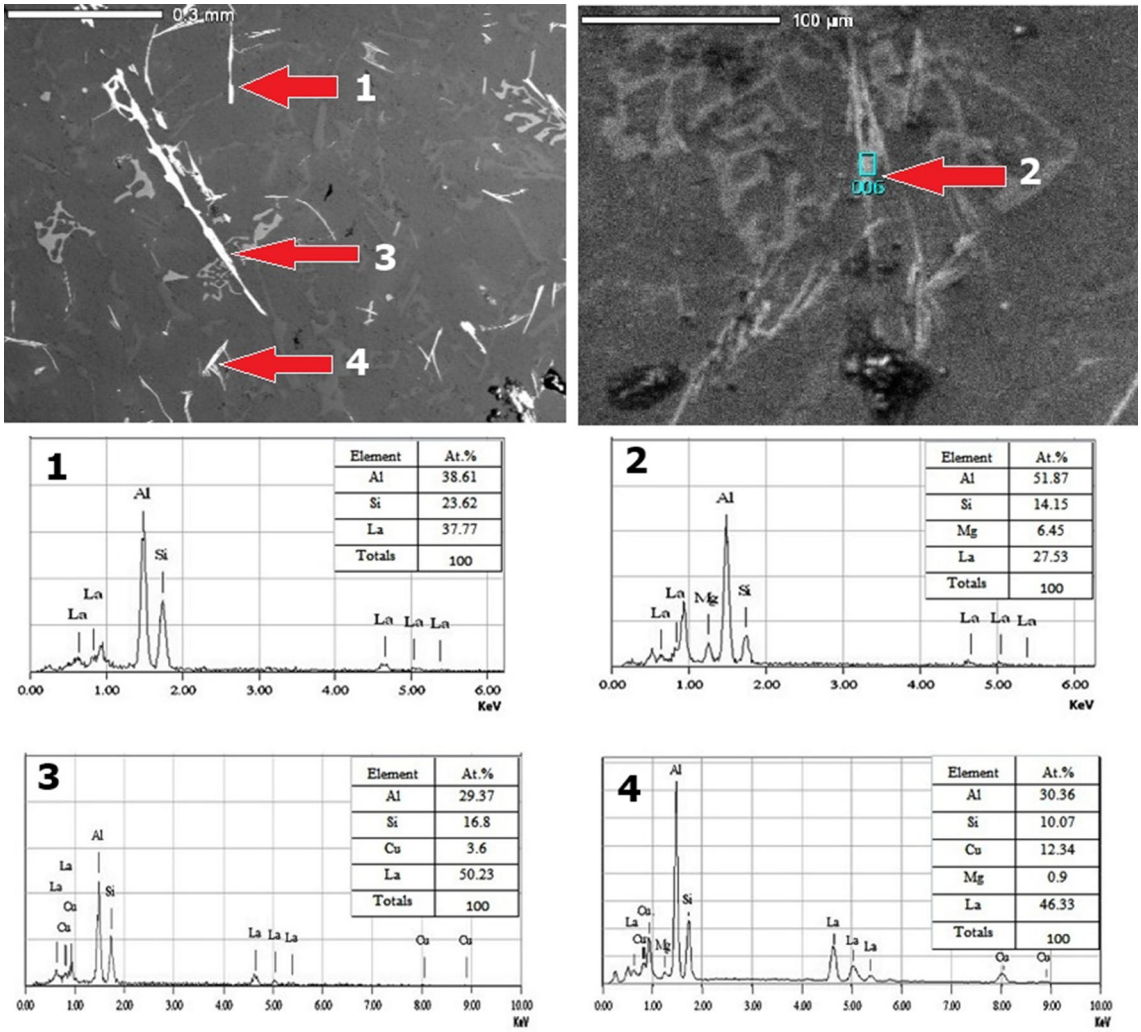

Fig. 12 SEM images and EDS analysis phases of location marked: (1) Al-Si-La, (2) Al-Si-Mg-La, (3) Al-Si-Cu-La, and (4) Al-Si-Mg-Cu-La

alloy, which may be partially due to the reappearance of harmful primary silicon cuboids with sharp-edged structures (Ref 57).

The elongation of the base alloy increased slightly with the La addition and reached 1.4% for all concentrations, except for 0.8 wt.%, and then increased for 1.0 wt.% La to 1.42%. This interruption of the elongation may due to the modification and intermetallic compound formation. Generally, the results of Al-Si-Cu-Mg with different La concentrations are consistent with those of A356 alloy supplemented by La, as reported by Tsai et al. (Ref 13).

The evaluation of the effect of the La concentration on the performance of the eutectic Al-Si-Cu alloy was performed using the quality index (Q). The quality index is described by Drouzy et al. (Ref 58) and modified by Closset and Gruzleski (Ref 59) as the semi-logarithmic plot of UTS versus elongation to fracture, Q = UTS + 150log El. As shown in Fig. 15, small amounts of 0.1 and 0.3 wt.% La increased Q from 215.2 to 228.4 and 225.8 MPa, respectively. When the value of La increases to more than 0.3 wt.%, Q did not improve. The additions of 0.5, 0.8, and 1.0 wt.% La yielded 214.4, 183.4, and 214.3 MPa, respectively. The quality index combines the strength and ductility and presents a description of the true tensile properties of the casting, rather than the tensile strength or elongation alone (Ref 13, 60). Hence, 0.1 wt.% La significantly improved the tensile strength and quality index of the Al-11Si-Cu-Mg cast alloy.

The SEM/EDS result indicated that the abundant La intermetallic compounds were larger than Si and harmful to the Si structure, where the compounds have a significant effect on the mechanical properties. A similar result was presented for the hypoeutectic Al-7Si-0.3 Mg alloy by Ravi et al. (Ref 12); the decrease in mechanical properties with the increasing mischmetal addition can be ascribed to the reaction of mischmetal with Mg to form complex compounds, leading to a reduction in the amount of free Mg available to form Mg_2Si. Thus, the RE-modified Al-Si-Cu-Mg alloy influenced the tensile properties. The formation of RE-containing intermetallic compounds decreased the tensile properties of the Al-Si alloy (Ref 14, 21). Yu-Chou et al. (Ref 21) ascribed this phenomenon to the following two factors: (1) grain coarsening and (2) the formation of RE-containing intermetallic compounds in the hypoeutectic Al-7Si-0.3 Mg alloy. With regard to the elongation to fracture, the results show that this parameter improved with the addition of La.

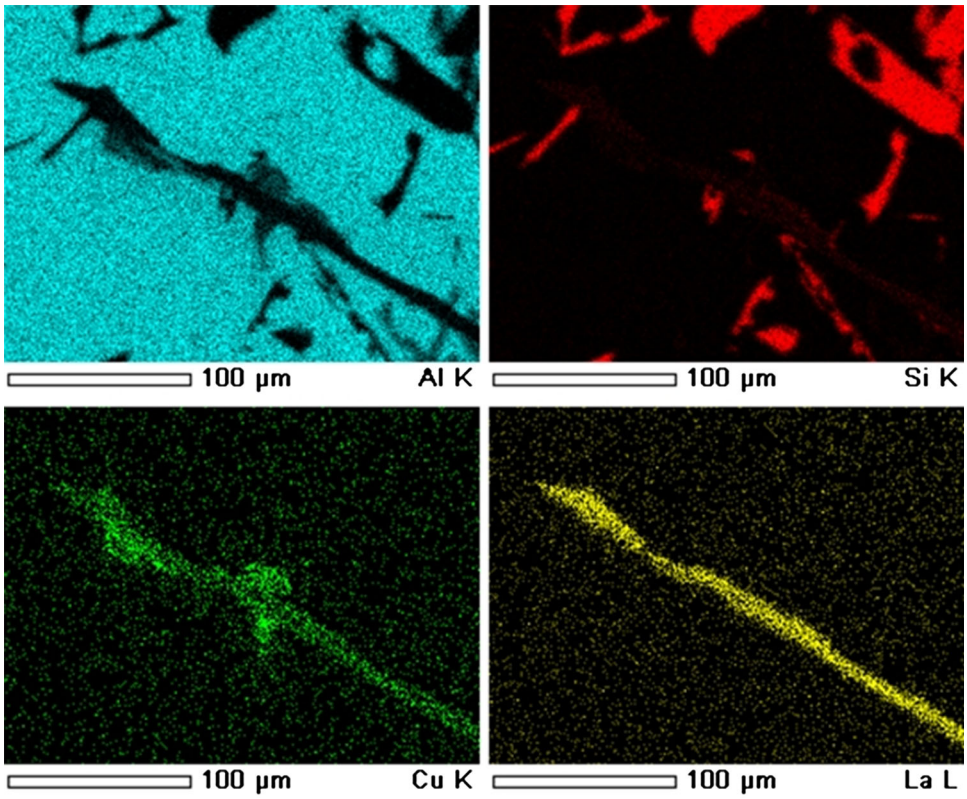

Fig. 13 EDS mapping of Al-Cu-La-Si phase

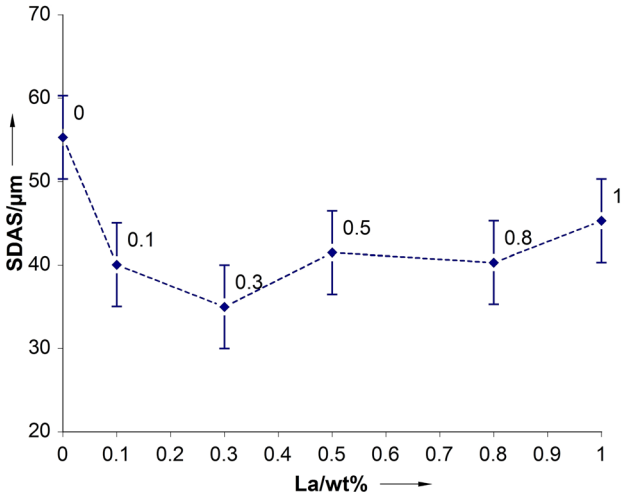

Fig. 14 Variation in the SDAS of Al-11Si-Cu-Mg as a function of the La addition

3.3.2 Fracture Surfaces. Figure 16 shows the fracture surfaces of the various alloys tested. At unmodified and lower La concentrations of 0.1 and 0.3 wt.%, the fracture surfaces were covered mainly by the cleavage plane. When the amount of La increased to 0.5 and 0.8 wt.%, the fracture surfaces were covered by cleavage planes and some dimples. Many dimples in the alloy with 1.0 wt.% showed a hollowed bottom, indicating that the extended plastic deformation involved in their formation and coalescence. The fracture surfaces of the tensile specimens indicated a brittle failure type for base alloys and alloys added with 0.1 and 0.5 wt.% La and a ductile failure mode in alloys supplemented with 0.8 and 1.0 wt.% La. However, the 0.8 wt.% La-containing alloy exhibited a lower elongation compared to that of other modified alloys. This phenomenon could be related to the irregular-shaped, longitudinal sharp edges of the Si structure, which leads to the widening of the existing microcracks during the elongation (Ref 14).

A similar result was obtained in the hypoeutectic Al-7Si-0.3 Mg alloy with different levels of La by Tsai et al. (Ref 13). Moreover, the fracture morphology of intergranular failure was mainly due to the coarse primary Si because the flow stress increased in the matrix and led to a higher level of stress transfer to the primary Si crystals in tensile testing. Therefore, fracture occurred in the primary Si when the tensile stress exceeded the intrinsic fracture stress of primary Si. In addition, the cracks primarily initiated and propagated along the interfaces between primary Si crystals and the aluminum matrix; then, neighboring cracks were linked, causing the fracture of materials in Al-Si alloys (Ref 48).

3.3.3 Hardness Test. The type, size, and distribution of the hardening phases formed during solidification depend to a great extent on the chemical composition of the alloy and alloying additives. In addition, the distribution of the Si particles and the intermetallic phases present in the microstructure play a vital role in determining the hardness and strength values of the aluminum-silicon casting alloys (Ref 36). The modification of the morphology of Si particles in the case of the non-modified samples would result in an increase in the hardness values of the as-cast alloys.

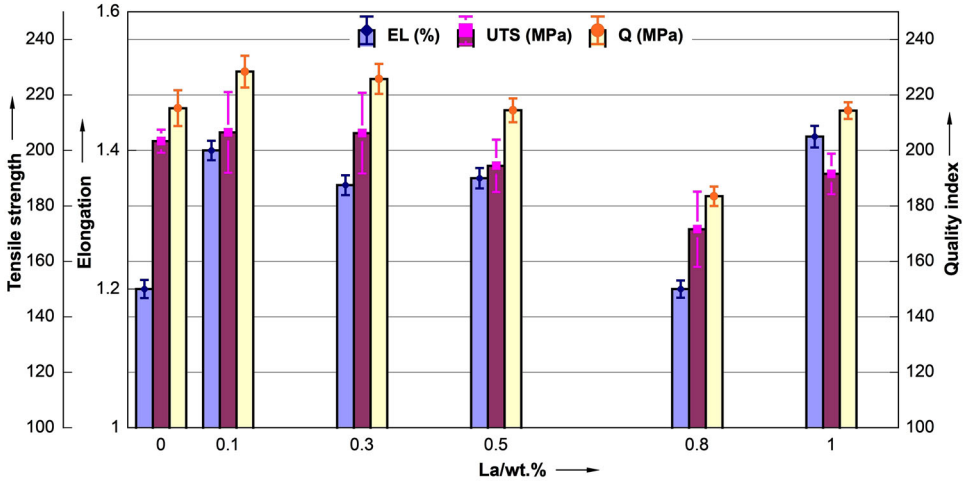

Fig. 15 Variation in means of UTS, elongation, and quality index of the as-cast Al-11Si-Cu-Mg alloys with and without La addition

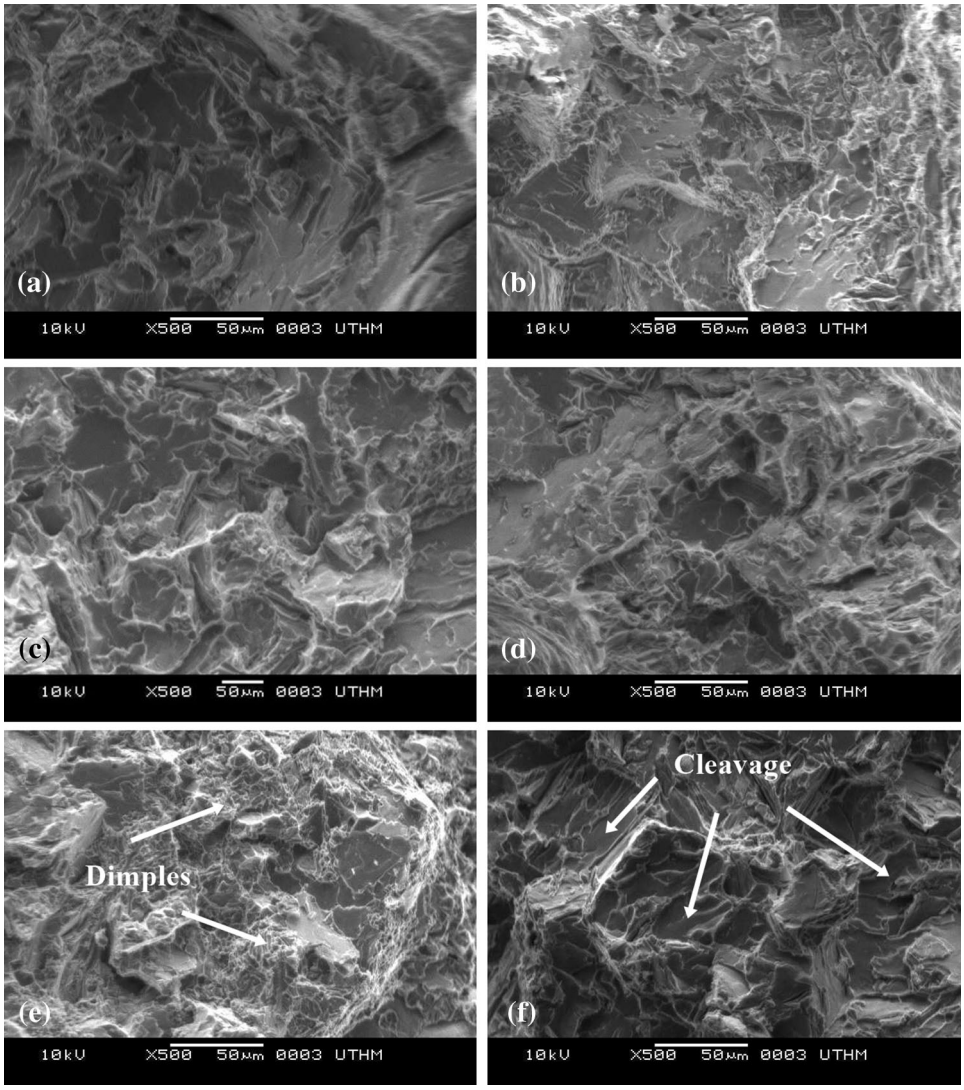

Fig. 16 Fracture surfaces of base Al-11Si-Cu-Mg with different La levels

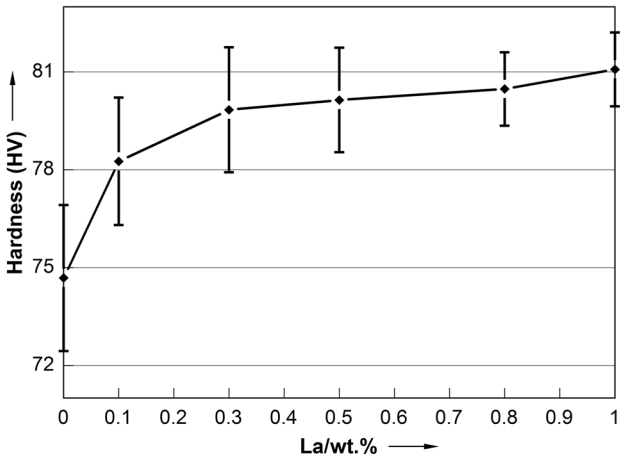

Fig. 17 Hardness value for base Al-11Si-Cu-Mg with different La levels

Figure 17 shows the hardness value for the base alloy and the alloys supplemented with different amounts of La. The additions of 0.1 and 0.3 wt.% La increased the hardness, with values of 78 and 79 HV, respectively, and slightly increased with the increasing amount of La added. Moreover, the hardness increased to 81 HV for 1.0 wt.% La. The analysis of the thermal properties and microstructure showed that La significantly influenced the solidification phases of Al-Si-Cu-Mg because of the high ability of La to react, thereby forming intermetallic compounds with other alloy elements. Hence, the increase in hardness with the increasing amount of La added is because of the formation of hard intermetallic compounds. In addition, the higher values of hardness obtained for La alloys may be ascribed to the fact that these alloys possess better combinations of the modified Si structure with a soft α-Al matrix (Ref 61). In addition, the effect of La on the α-Al phase formed harder intermetallic compounds, such as $LaAl_4$ (Ref 62, 63).

The increment in the microhardness of the hypoeutectic Al-7Si-0.3 Mg alloy is due to the increase in the quantity of the relatively hard-phase Al-La present, as reported by Ravi et al. (Ref 12). Furthermore, the La addition formed hard intermetallic compounds with other alloying elements in the matrix and consumed a certain amount of Mg for the formation of these compounds (Ref 12, 61). As obtained in the EDS result, the La addition leads to the formation of the Mg_2Si phase and the intermetallic compound Al-Si-Mg-La and varied widely with the increasing level of addition. The results of the hardness test of the Al-11Si-Cu-Mg eutectic alloy with different levels of La are in agreement with the findings of Ravi et al. (Ref 12) and El Sebaie et al. (Ref 61). In addition, the refinement of SDAS at the α-Al phase with the addition of La increased the hardness (Ref 64).

4. Conclusions

A detailed investigation was conducted to determine the effect of La addition on the solidification, microstructure, and mechanical properties of eutectic Al-Si-Cu-Mg cast alloy. The following conclusions can be drawn from the experimental results:

(1) The growth ($T_G^{Al\text{-}Si}$) and nucleation ($T_N^{Al\text{-}Si}$) temperatures decreased to 569.8 and 571.4 °C, respectively, as the amount of La increased to 1.0 wt.%. In addition, the recalescence temperature increased with the increasing level of La; thus, the value of the depression increased when the amount of La added increased to 1.0 wt.%.

(2) The refiner structure of Si particles was observed through microstructure analysis. La addition decreased the size of Si particles to 21 μm^2 at high levels of La (1.0 wt.%).

(3) La addition significantly affects the final stages of the Al-Cu solidification phase. The increment of the La addition amount (1.0 wt.% La) leads to higher growth $T_G^{Al\text{-}Cu}$ and nucleation $T_N^{Al\text{-}Cu}$ temperatures of Al-Cu.

(4) Secondary or tertiary compounds formed by La with alloy elements, such as Al, Si, Cu, and Mg, as well as the formed compounds, such as Al-Si-La, Al-Si-Mg-La, Al-Si-Cu-La, and Al-Si-Mg-Cu-La, appear needle-like and are uniform and randomly distributed in the modified Si.

(5) The results of the solidification parameters indicate that La addition has a significant effect on the SDAS value, while the SDAS was refined approximately 35-40 μm with La addition due to the reduction time of the α-Al phase and solidification range.

(6) The tensile strength and quality index of the base alloy increased to 206.5 and 228.4 MPa, respectively, after the addition of 0.1 wt.% La, while the elongation mostly increased to 1.4% with La addition, except for in the 0.8 wt.% La-containing alloy. The hardness of the eutectic Al-Si-Cu-Mg alloy increased continuously with the increasing La concentration.

Acknowledgments

The authors would like to acknowledge the Ministry of Higher Education Malaysia and Universiti Tun Hussein Onn Malaysia for supporting this research under Vot no FRGS1422 and E15501.

References

1. V.S. Zolotorevsky, N.A. Belov, and M.V. Glazoff, *Casting Aluminum Alloys*, Elsevier, Oxford, 2010
2. C.T. Rios, R. Caram, and C. Bolfarini, Intermetallic Compounds in the Al-Si-Cu System, *Acta Microsc*, 2003, **12**, p 77–81
3. N. Alexopoulos and S.G. Pantelakis, Evaluation of the Effects of Variations in Chemical Composition on the Quality of Al-Si-Mg, Al-Cu, and Al-Zn-Mg Cast Aluminum Alloys, *J. Mater. Eng. Perform.*, 2003, **12**, p 196–205
4. E. Wang, X. Hui, and G. Chen, Eutectic Al-Si-Cu-Fe-Mn Alloys with Enhanced Mechanical Properties at Room and Elevated Temperature, *Mater. Des.*, 2011, **32**, p 4333–4340
5. S. Manasijevic, R. Radisa, S. Markovic, Z. Acimovic-Pavlovic, and K. Raic, Thermal Analysis and Microscopic Characterization of the Piston Alloy AlSi13Cu4Ni2Mg, *Intermetallics*, 2011, **19**, p 486–492
6. K.A. Gschneidner, J.-C. Bünzli, and V.K. Pecharsky, *Handbook on the Physics and Chemistry of Rare earths*. Access Online via Elsevier, 2004
7. D.K. Dwivedi, A. Sharma, and T. Rajan, Influence of Silicon Morphology and Mechanical Properties of Piston Alloys, *Mater. Manuf. Process.*, 2005, **20**, p 777–791
8. H. Zahedi, M. Emamy, A. Razaghian, M. Mahta, J. Campbell, and M. Tiryakioğlu, The Effect of Fe-Rich Intermetallics on the Weibull Distribution of Tensile Properties in a Cast Al-5 Pct Si-3 Pct Cu-1 Pct Fe-0.3 Pct Mg Alloy, *Metall. Mater. Trans. A*, 2007, **38**, p 659–670

9. J.G. Kaufman and E.L. Rooy, *Aluminum Alloy Castings: Properties, Processes, and Applications*, ASM International, Materials Park, 2004
10. R. Sharan and N. Saksena, Rare-Earth Additions to Aluminum-Silicon Alloys, *Castings*, 1978, **24**, p 37–41
11. B. Ye, C. Loper, D. Lu, and C. Kang, An Assessment of the Role of Rare Earth in the Eutectic Modification of Cast Aluminum-Silicon Alloys, *AFS Trans.*, 1985, **93**, p 533–544
12. M. Ravi, U. Pillai, B. Pai, A. Damodaran, and E. Dwarakadasa, A Study of the Influence of Mischmetal Additions to Al-7Si-0.3 Mg (LM 25/356) Alloy, *Metall. Mater. Trans. A*, 1996, **27**, p 1283–1292
13. Y.C. Tsai, C.Y. Chou, S.L. Lee, C.K. Lin, J.C. Lin, and S. Lim, Effect of Trace La Addition on the Microstructures and Mechanical Properties of A356 (Al-7Si-0.35 Mg) Aluminum Alloys, *J. Alloys Compd.*, 2009, **487**, p 157–162
14. M. Zhu, Z. Jian, L. Yao, C. Liu, G. Yang, and Y. Zhou, Effect of Mischmetal Modification Treatment on the Microstructure, Tensile Properties, and Fracture Behavior of Al-7.0% Si-0.3% Mg Foundry Aluminum Alloys, *J. Mater. Sci.*, 2011, **46**, p 2685–2694
15. H. Yi and D. Zhang, Morphologies of Si Phase and La-Rich Phase in As-Cast Hypereutectic Al-Si-xLa Alloys, *Mater. Lett.*, 2003, **57**, p 2523–2529
16. J.F. Chen and J.J. Yang, Modification Mechanism of Rare Earth La in Al-Si Alloy, *Foundry Technol*, 2008, **5**, p 031
17. H. Yi, D. Zhang, T. Sakata, and H. Mori, Microstructures and La-Rich Compounds in a Cu-Containing Hypereutectic Al-Si Alloy, *J. Alloys Compd.*, 2003, **354**, p 159–164
18. A. Canales, J. Talamantes-Silva, D. Gloria, S. Valtierra, and R. Colás, Thermal Analysis During Solidification of Cast Al-Si Alloys, *Thermochim. Acta*, 2010, **510**, p 82–87
19. A. Niklas, U. Abaunza, and J. Lacaze, Relationship Between Casting Modulus and Grain Size in Cast A356 Aluminium Alloys, *IOP Conf. Ser. Mater. Sci. Eng*, IOP Publishing, 2012, p 012003
20. M. Ghoncheh, S. Shabestari, and M. Abbasi, Effect of Cooling Rate on the Microstructure and Solidification Characteristics of Al2024 Alloy Using Computer-Aided Thermal Analysis Technique, *J. Therm. Anal. Calorim.*, 2014, **117**, p 1253–1261
21. Y.C. Tsai, S.L. Lee, and C.K. Lin, Effect of Trace Ce Addition on the Microstructures and Mechanical Properties of A356 (AL-7SI-0.35 Mg) Aluminum Alloys, *J. Chin. Inst. Eng.*, 2011, **34**, p 609–616
22. S. Farahany, M.H. Idris, A. Ourdjini, F. Faris, and H. Ghandvar, Evaluation of the Effect of Grain Refiners on the Solidification Characteristics of an Sr-Modified ADC12 Die-Casting Alloy by Cooling Curve Thermal Analysis, *J. Therm. Anal. Calorim*, 2015, **119**, p 1593–1601
23. S. Farahany, A. Ourdjini, T.A.A. Bakar, and M.H. Idris, A New Approach to Assess the Effects of Sr and Bi Interaction in ADC12 Al-Si Die Casting Alloy, *Thermochim. Acta*, 2014, **575**, p 179–187
24. S. Farahany, A. Ourdjini, M. Idrsi, and S. Shabestari, Evaluation of the Effect of Bi, Sb, Sr and Cooling Condition on Eutectic Phases in an Al-Si-Cu Alloy (ADC12) by In-Situ Thermal Analysis, *Thermochim. Acta*, 2013, **559**, p 59–68
25. S. Shabestari and M. Malekan, Assessment of the Effect of Grain Refinement on the Solidification Characteristics of 319 Aluminum Alloy Using Thermal Analysis, *J. Alloys Compd.*, 2010, **492**, p 134–142
26. D. Neff, *Improving Die Casting Melt Quality and Casting Results with Melt quality Analysis and filtration*, Metaullics Systems Co., Solon, OH, 2014
27. M.R.V. Vijeesh and K. Prabhu, The Effect of the Addition of Strontium and Cerium Modifiers on Microstructure and Mechanical Properties of Hypereutectic Al-Si (LM30) Alloy, *Mater. Perform. Charact.*, 2013, **2**, p 296–307
28. L. Bäckerud, G. Chai, and J. Tamminen, *Solidification Characteristics of Aluminum Alloys*, AFS/Skanaluminium, Des Plaines, 1990
29. A. Knuutinen, K. Nogita, S. McDonald, and A. Dahle, Modification of Al-Si Alloys with Ba, Ca, Y and Yb, *Light Met.*, 2001, **1**, p 229–240
30. C. Gonzalez-Rivera, J. Baez, R. Chavez, A. Garcıá, and J. Juarez-Islas, Quantification of the SiCp Content in Molten Al-Si/SiCp Composites by Computer Aided Thermal Analysis, *J. Mater. Process. Technol.*, 2003, **143–144**, p 860–865
31. S. Farahany, A. Ourdjini, M. Idris, and S. Shabestari, Computer-Aided Cooling Curve Thermal Analysis of Near Eutectic Al-Si-Cu-Fe Alloy, *J. Therm. Anal. Calorim*, 2013, **114**, p 705–717
32. J. Li and P. Schumacher, Effect of Y Addition and Cooling Rate on Refinement of Eutectic Si in Al-5 wt-% Si Alloys, *Int. J. Cast Met. Res.*, 2012, **25**, p 347–357
33. S. Farahany and A. Ourdjini, Effect of Cooling Rate and Silicon Refiner/Modifier on Solidification Pathways of Al-11.3Si-2Cu-0.4Fe Alloy, *Mater. Manuf. Process.*, 2013, **28**, p 657–663
34. T. Ludwig, E.S. Dæhlen, P. Schaffer, and L. Arnberg, The Effect of Ca and P Interaction on the Al-Si Eutectic in a Hypoeutectic Al-Si Alloy, *J. Alloys Compd.*, 2014, **586**, p 180–190
35. M. Ibrahim, E. Samuel, A. Samuel, A. Al-Ahmari, and F. Samuel, Impact Toughness and Fractography of Al-Si-Cu-Mg Base Alloys, *Mater. Des.*, 2011, **32**, p 3900–3910
36. M. Ibrahim, E. Samuel, A. Samuel, A. Al-Ahmari, and F. Samuel, Metallurgical Parameters Controlling the Microstructure and Hardness of Al-Si-Cu-Mg Base Alloys, *Mater. Des.*, 2011, **32**, p 2130–2142
37. S. Shabestari and S. Ghodrat, Assessment of Modification and Formation of Intermetallic Compounds in Aluminum Alloy Using Thermal Analysis, *Mater. Sci. Eng. A*, 2007, **467**, p 150–158
38. B. Pourbahari and M. Emamy, Effects of La Intermetallics on the Structure and Tensile Properties of Thin Section Gravity Die-Cast A357 Al Alloy, *Mater. Des.*, 2016, **94**, p 111–120
39. W. Jiang, Z. Fan, Y. Dai, and C. Li, Effects of Rare Earth Elements Addition on Microstructures, Tensile Properties and Fractography of A357 Alloy, *Mater. Sci. Eng. A*, 2014, **597**, p 237–244
40. H. Qiu, H. Yan, and Z. Hu, Effect of Samarium (Sm) Addition on the Microstructures and Mechanical Properties of Al-7Si-0.7 Mg Alloys, *J. Alloys Compd.*, 2013, **567**, p 77–81
41. J.M. Boileau and J.E. Allison, The Effect of Solidification Time and Heat Treatment on the Fatigue Properties of a Cast 319 Aluminum Alloy, *Metall. Mater. Trans. A*, 2003, **34**, p 1807–1820
42. J.M. Boileau, J.W. Zindel, and J.E. Allison, The Effect of Solidification Time on the Mechanical Properties in a Cast A356-T6 Aluminum Alloy, *Power*, 1997, **2013**, p 07–15
43. A. Mohamed and F. Samuel, A Review on the Heat Treatment of Al-Si-Cu/Mg casting alloys, 2012, *Heat Treatment—Conventional and Novel Applications*, InTech, 2012, p 229
44. J. Chang, I. Moon, and C. Choi, Refinement of Cast Microstructure of Hypereutectic Al-Si Alloys Through the Addition of Rare Earth Metals, *J. Mater. Sci.*, 1998, **33**, p 5015–5023
45. S. Pramod, A.P. Rao, B. Murty, and S.R. Bakshi, Effect of Sc Addition on the Microstructure and Wear Properties of A356 Alloy and A356-TiB 2 In Situ Composite, *Mater. Des.*, 2015, **78**, p 85–94
46. F. Mao, G. Yan, Z. Xuan, Z. Cao, and T. Wang, Effect of Eu Addition on the Microstructures and Mechanical Properties of A356 Aluminum Alloys, *J. Alloys Compd.*, 2015, **650**, p 896–906
47. Q. Li, T. Xia, Y. Lan, W. Zhao, L. Fan, and P. Li, Effect of Rare Earth Cerium Addition on the Microstructure and Tensile Properties of Hypereutectic Al-20% Si Alloy, *J. Alloys Compd.*, 2013, **562**, p 25–32
48. Q. Li, T. Xia, Y. Lan, P. Li, and L. Fan, Effects of Rare Earth Er Addition on Microstructure and Mechanical Properties of Hypereutectic Al-20% Si Alloy, *Mater. Sci. Eng., A*, 2013, **588**, p 97–102
49. S.-Z. Lu and A. Hellawell, The Mechanism of Silicon Modification in Aluminum-Silicon Alloys: Impurity Induced Twinning, *Metall. Mater. Trans. A*, 1987, **18**, p 1721–1733
50. R. Mackay and J. Sokolowski, Effect of Si and Cu Concentrations and Solidification Rate on Soundness in Casting Structure in Al-Si-Cu Alloys, *Int. J. Cast Met. Res.*, 2010, **23**, p 7–22
51. S. Boontein, N. Srisukhumbovornchai, J. Kajornchaiyakul, and C. Limmaneevichitr, Reduction in Secondary Dendrite Arm Spacing in Cast Aluminium Alloy A356 by Sb Addition, *Int. J. Cast Met. Res.*, 2011, **24**, p 108–112
52. S. Yamanaka, S. Izumi, S. Maekawa, and K. Umemoto, Phase Diagram of the La-Si Binary System Under High Pressure and the Structures of Superconducting LaSi 5 and LaSi 10, *J. Solid State Chem.*, 2009, **182**, p 1991–2003
53. M. Vončina, S. Kores, P. Mrvar, and J. Medved, Effect of Ce on Solidification and Mechanical Properties of A360 Alloy, *J. Alloys Compd.*, 2011, **509**, p 7349–7355
54. Y. Chen, Y. Pan, T. Lu, S. Tao, and J. Wu, Effects of Combinative Addition of Lanthanum and Boron on Grain Refinement of Al-Si Casting Alloys, *Mater. Des.*, 2014, **64**, p 423–426
55. X. Hu, F. Jiang, F. Ai, and H. Yan, Effects of Rare Earth Er Additions on Microstructure Development and Mechanical Properties of Die-Cast ADC12 Aluminum Alloy, *J. Alloys Compd.*, 2012, **538**, p 21–27

56. G. An, L. Liu, and G. Gu, Effect of Ce on the Interface Stability and Dendrite Arm Spacing of Al-Cu Alloys, *J. Cryst. Growth*, 1987, **83**, p 96–100
57. H. Qiu, H. Yan, and Z. Hu, Modification of Near-Eutectic Al-Si Alloys with Rare Earth Element Samarium, *J. Mater. Res.*, 2014, **29**, p 1270–1277
58. M. Drouzy, S. Jacob, and M. Richard, Interpretation of Tensile Results by Means of Quality Index and Probable Yield Strength, *Int. J. Cast Met. Res.*, 1980, **5**, p 43–50
59. B. Closset and J. Gruzleski, Mechanical Properties of A356.0 Alloys Modified with Pure Strontium, *AFS Trans*, 1982, **31**, p 453–464
60. S. Farahany, M.H. Idris, and A. Ourdjini, Effect of Bismuth and Strontium Interaction on the Microstructure Development, Mechanical Properties and Fractography of a Secondary Al-Si-Cu-Fe-Zn Alloy, *Mater. Sci. Eng. A*, 2015, **621**, p 28–38
61. O. El Sebaie, A. Samuel, F. Samuel, and H. Doty, The Effects of Mischmetal, Cooling Rate and Heat Treatment on the Hardness of A319.1, A356.2 and A413.1 Al-Si Casting Alloys, *Mater. Sci. Eng. A*, 2008, **486**, p 241–252
62. Y. Chen, Q. Li, and Z. Jiang, Influence of Cerium and Mischmetal on the Hardness and Brightness of Al-1%Mg-0.5%Si Alloys, *J. Less-Common Met.*, 1985, **110**, p 175–178
63. M. Zhang, X. Meng, R. Wu, C. Cui, and L. Wu, Effect of Ce on Microstructures and Mechanical Properties of As-Cast Mg-8Li-1Al Alloys, *Kovove Mater.*, 2010, **48**, p 211–216
64. Z.R. Nie, T. Jin, J. Fu, G. Xu, J. Yang, J.X. Zhou, and T.Y. Zuo, Research on Rare Earth in Aluminum, *Mater. Sci. Forum*, 2002, **396**, p 1731